Application of the Total Focusing Method for Improved Defect Characterization in the Production of Steel Tubes, Pipes and Plates

Till SCHMITTE [1], Oliver NEMITZ [1], Nikolai CHICHKOV [1], Thomas ORTH [1]
[1] Salzgitter Mannesmann Forschung GmbH, Duisburg, Germany

Contact e-mail: t.schmitte@du.szmf.de
Ehinger Straße 200, 47259 Duisburg, Germany

Abstract. TFM, SAFT, and other imaging techniques provide intuitive, interpretable results and high signal-to-noise ratios. So far, the computational complexity of these methods limits the number of possible applications and prevents wide-spread transfer to production environments. In this paper we will introduce a new TFM-system, developed by SZMF, which has been designed for time-efficient inspection of steel components after production.

The presented TFM-system supports different interfaces between coupling medium and steel, among them a circular interface to allow for the curvature of pipes. Arbitrary combinations of sending and/or receiving elements can be chosen. Anisotropic sound velocities, common in rolled steel, are taken into account to further improve reconstruction quality and reduce artifacts. Finally, to achieve significantly reduced TFM-reconstruction times, the computational kernel is implemented in CUDA C on a GPU.

1. Introduction

Imaging techniques like TFM and SAFT have become quite popular over the past years, as they provide intuitive, interpretable results and high signal-to-noise ratios. The progress in computer technology, especially of FPGAs and GPUs, nowadays cope with the high computational complexity of these methods, which makes imaging with acceptable frame rates possible. Nevertheless, the development of such imaging systems for production environments is still an ongoing process.

In this paper, we will introduce a new TFM-system, developed by SZMF, which has been designed for the inspection of steel components during production. Special demands of our customers, like consideration of material anisotropy, curved surfaces, and others, are already implemented or work in progress.

The basic TFM algorithm is for example explained in [**1**], an overview about several ways to analyse the measured full matrix capture (FMC) can be found in [**2**]. The aim of these methods is to have a better defect characterization, which includes the position, size, and shape of the defects.

2. SZMF TFM Implementation

In order to adjust the TFM algorithm according to the demands of our customers, we developed our own implementation in Matlab. Although Matlab programs are not very fast, the powerful and easy to use language gives us the possibility to quickly realise and test new approaches and features. Most modifications can easily be implemented and the visualization possibilities allow for fast debugging and verification of computations and algorithms.

The core computational kernel of the reconstruction algorithm is implemented in CUDA C on a GPU (see section 3). Utilising transmitting and receiving element sparsity is another way of gaining speed (see section 4). Section 5 deals with our sector grid implementation, followed by the description of handling circular interfaces in section 6. The consideration of material anisotropy is regarded (section 7) and the more complete reconstruction of reflectors using half- and full-skip TFM is treated thereafter (section 8). The paper concludes with a section about defect sizing (section 9) and a short outlook (section 10).

All TFM reconstruction images in this paper have been processed with a column wise Hilbert transform. For all measurements we used the MicroPulse 5PA device from PeakNDT.

3. CUDA C Implementation on a GPU

The conventional TFM algorithm can be implemented with three nested for-loops (over all transmitters, grid cells, and receivers). In each transmitter-cell-receiver combination the time-of-flight from transmitter to grid cell to receiver is computed, the corresponding amplitude is extracted from the Full Matrix Capture (FMC) and added to the reconstruction image. These computations can be performed independently for each of these combinations.

Hence, to significantly increase speed of the TFM reconstruction algorithm, an implementation on a graphics card, where hundreds of kernels run in parallel, is very appropriate (see [**3**] for Paintbrush and [**4**] for TFM on a GPU). We implemented the computational kernel in Cuda C and called it via a Mex interface from our Matlab GUI. The used graphics card was an Nvidia Geforce GTX 670 with 1344 cores á 915 MHz and 2 GB of memory. With a price of about 340 € in 2012 it was not even a high-end gamer graphics card. Nevertheless, it was possible to reduce the reconstruction time by a factor of about 40 compared to a core “C” implementation (not the Matlab implementation).

4. Sparsity

Another way of reducing the execution time of the TFM algorithm is to make use of probe sparsity (see for example [**5**] and [**6**]). Instead of transmitting and receiving with all phased-array probe elements, it is possible to use only a certain subset of elements. For example, shooting only with every second, but still receiving with all elements, already halves the amount of data and the reconstruction time. Shooting and receiving with only every second element quarters the amount of data, as well as the reconstruction time. In our implementation the usage of sparsity for transmitting, as well as for receiving elements is possible.

Of course, this results in a lower reconstruction image quality, but depending on the application, the element pitch, and the grid size this can be negligible. In Figure 1 we tested the reconstruction quality of different grades of sparsity of sending elements. A sample

with five through drilled holes of 2 mm diameter and a 64 element 5 MHz phased array probe with 0.6 mm pitch have been used. One can observe that in this example, it is possible to reduce the number of sending elements up to a certain degree, without significantly losing image quality. Only higher sparsity leads to a clear SNR drop and distortions in the reconstruction image.

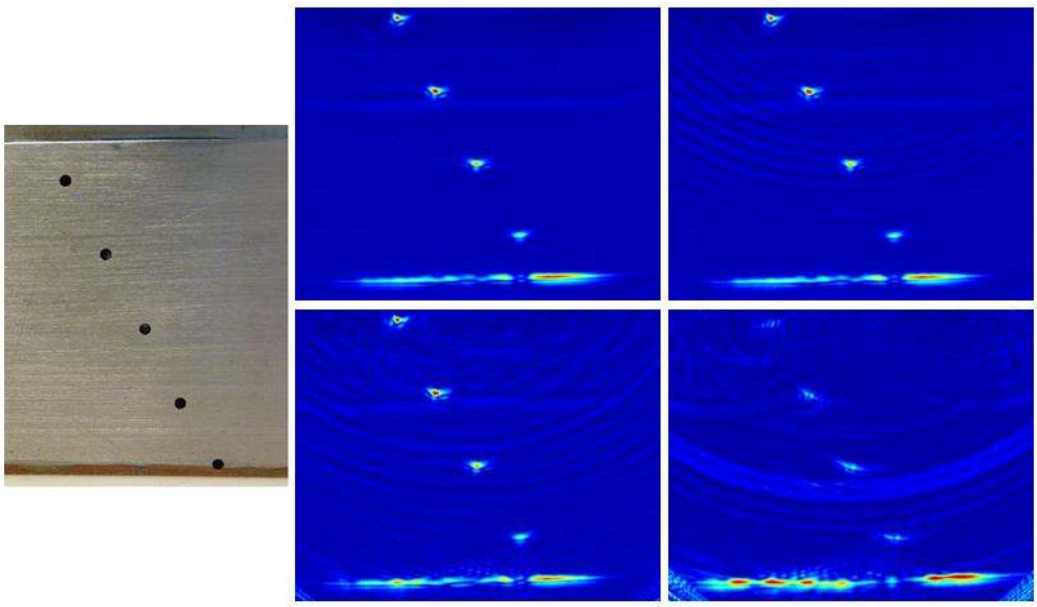

Figure 1: Examples of TFM reconstructions of a sample with five through drilled holes (top left) with different grades of sending sparsity. Top row, from left to right: sample, usual TFM construction with all elements, reconstruction only with every second sending element. Bottom row, from left to right: reconstruction with every eighth, every 32nd element and finally with the first and last element only.

5. Different Grids: Rectangular and Sector Grid

In some applications, e.g. weld inspections, the region of interest is not inspected directly from top of the sample but under a certain angle. Often, a wedge is used to steer the main intensity propagation direction of the waves into a predefined direction. In such cases, a grid formed like a sector scan can describe the region where significant wave propagation takes place more intuitively. Furthermore, a computation in regions where the wave has almost no intensity is not necessary. This saves grid cells and computation time orallows a finer resolution with the same number of cells. In Figure 2 such a grid is shown and compared to a usual phased array sector scan.

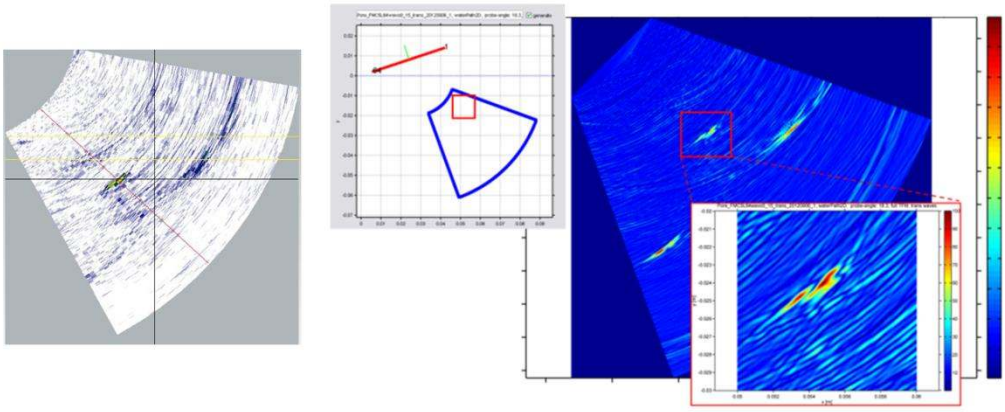

Figure 2: Left: visualization of a conventional sector scan, right: using not a rectangular but a sector grid in our software.

6. Curved Interfaces

The TFM algorithm is easy to implement if the phased array probe is in direct contact with a flat specimen surface. In that case, the distance from one probe element to one grid cell is simply the length of the direct connection line. If there is a water path or a wedge, the specimen surface describes an interface between steel and water, (or wedge material, respectively) where the ultrasonic beam is refracted. Hence, to compute the time-of-flight between grid cells and probe elements, it is necessary to know the correct intersection points on this interface. These points can be derived with Fermat's principle, which simply states that a beam will travel along the path of the smallest time-of-flight. For a planar interface this leads to a fourth order polynomial equation (see [7]), which can be solved analytically with Cardano's formulas. In case of pipe inspections, the interface is described by a circle, which leads to a 6^{th} order equation, which cannot be solved analytically anymore. Hence, in our implementation we use a numerical approach to minimize the time-of-flights, which results in the intersection points on such a circular interface. In Figure 3 the influence of a correct consideration of curved surfaces is demonstrated.

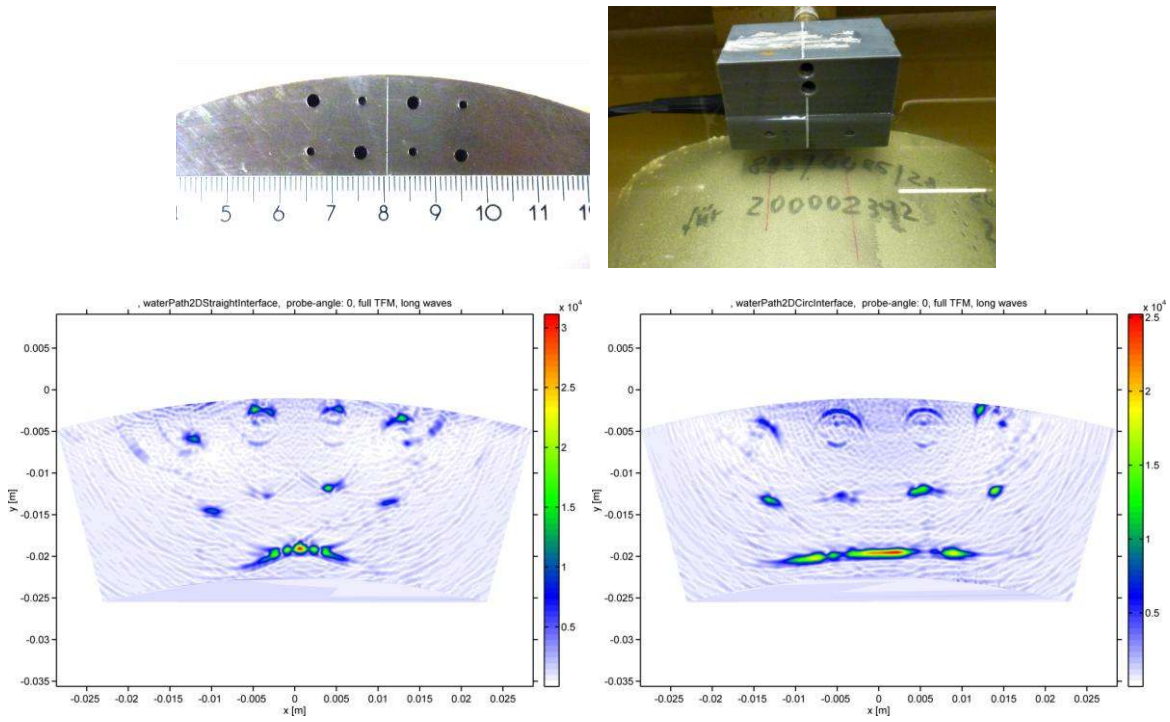

Figure 3: Experimental validation of the intersection point computation on a circular interface. The 64 elements phased array probe with 5 MHz (already described in section) is placed in a distance of 20 mm to a probe sample of dimension 223x21 mm in which eight holes of 1 and 2 mm diameter have been drilled (top row). In the bottom row on the left a TFM reconstruction with an assumed planar interface (tangential at the top of the pipe) is shown. The resulting image is distorted which is not the case if a circular interface is used (right-hand side).

7. Material Anisotropy

In some materials, e.g. rolled steel plates, the ultrasound velocity depends on the beam direction, i.e. the material exhibits anisotropic characteristics. This circumstance does not only complicate the computation of time-of-flights for known intersection points but especially the determination of the intersection points themselves.

As we have to deal with such materials in our applications, we implemented the computation of intersection points and time-of-flights for anisotropic materials for both planar and circular interfaces. The intersection points have been determined by minimizing

the time-of-flight numerically (Fermat's principle). Minimization algorithms implemented in C++ as Mex functions ensure that the computation can be performed within a few seconds. In our usual applications the computation of intersection points can be performed once in advance - waiting a few seconds for a pre-computation is acceptable there. In situations where the intersection points have to be computed in real time, maybe because the phased array probe moves along a changing specimen surface, it would be possible to also gain speed by implementing these algorithms on a GPU.

In Figure 4 the effect of the anisotropy consideration can clearly be seen: without it the TFM reconstruction of a side drilled hole is smeared and exhibits a low signal-to-noise ratio. With the consideration of anisotropy the reconstruction of the drilled hole is much more focused and the SNR is significantly higher.

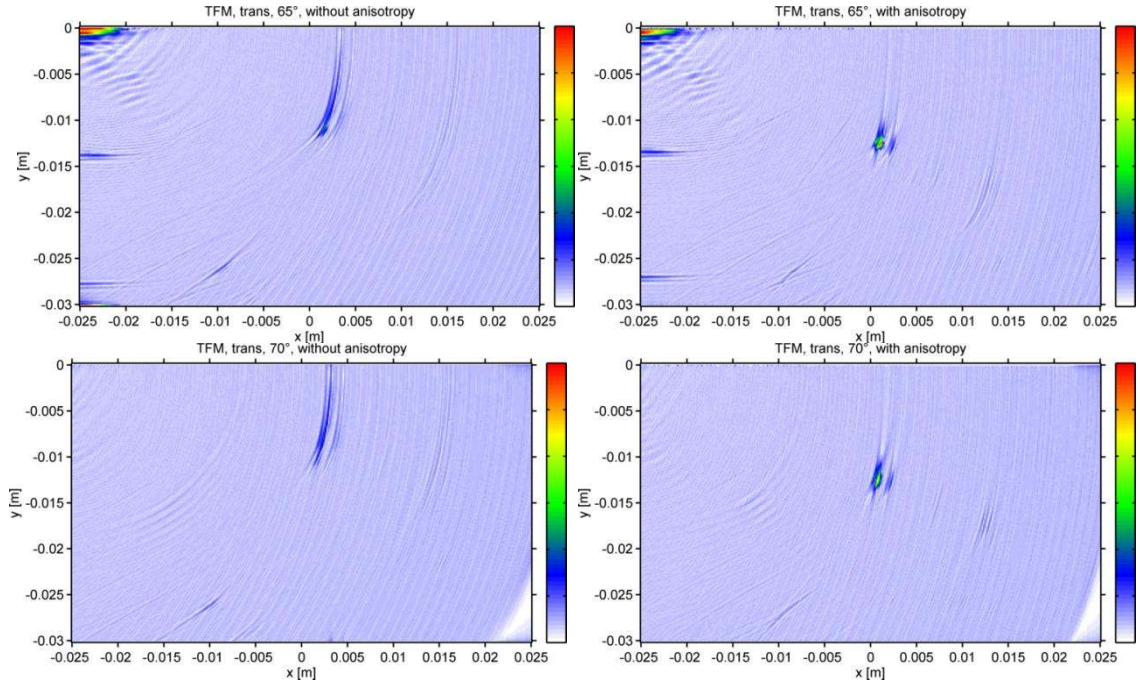

Figure 4: Effects of anisotropic considerations: Top row: TFM reconstruction of a 1mm drill hole in a rolled steel plate with 25 mm wall thickness under the incidence angle of 65° without (left) and with (right) consideration of anisotropy. Bottom row: TFM reconstruction of the same sample on the incidence angle of 70° without (left) and with (right) consideration of anisotropy.

8. Half and Full Skip TFM

The conventional TFM algorithm can only reconstruct that part of a reflector which is facing the phased array probe. For a more complete description of the reflector it is possible to also regard those beams which have been reflected at the backwall of the sample (see [**11**], [**12**], [**13**]). This is possible with two different types of skips (cf. Figure 5). In the so-called half-skip TFM the beam from one element (either transmitter or receiver) is reflected at the backwall whereas the other beam directly runs from the grid cell to the other probe element. In the full-skip TFM both these beams are reflected at the backwall. These two approaches can simultaneously be used in addition to the conventional TFM. The final reconstruction image is then just the (possibly weighted) sum of the single reconstruction images.

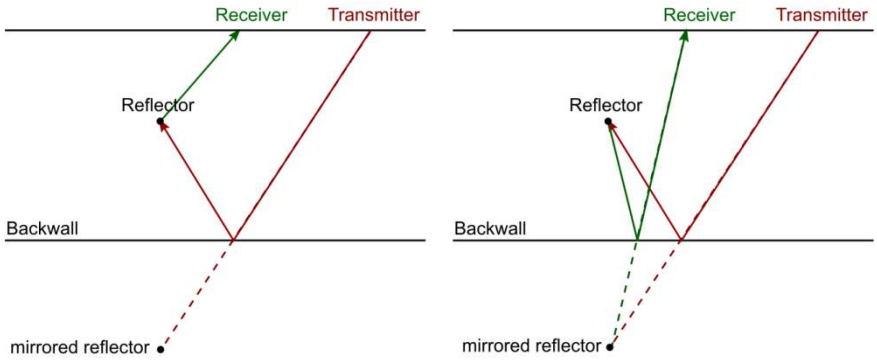

Figure 5: Left: Half-skip TFM: One beam is reflected at the backwall, the other runs directly from reflector to probe element. Right: Full-skip TFM: Both beams are reflected at the backwall.

Half-Skip and Full-Skip TFM with a Planar Backwall

If the backwall is planar, the time-of-flight from a probe element to a grid cell including backwall reflection just corresponds to the time-of-flight from the probe element to the grid cell mirrored at the backwall (cf. Figure 5). The reflector at this mirrored position can also be seen as a virtual transducer corresponding to the original reflector position. In the planar case and for one fix grid cell its position is constant for all probe element positions.

Therefore, it is possible here to extend the reconstruction domain by a certain region below the backwall and to perform the usual TFM reconstruction on this extended domain. Afterwards, the reconstruction in this new region can simply be mirrored at the backwall and added to the former reconstruction region above the backwall. In Figure 6 the difference between the conventional and the full skip TFM applied to a steel block with 5 mm through drilled holes is shown. In the conventional TFM reconstruction only the upper side of the hole is reconstructed whereas in the full skip TFM also a part of the lower side is visible (in the distance of approximately 5 mm).

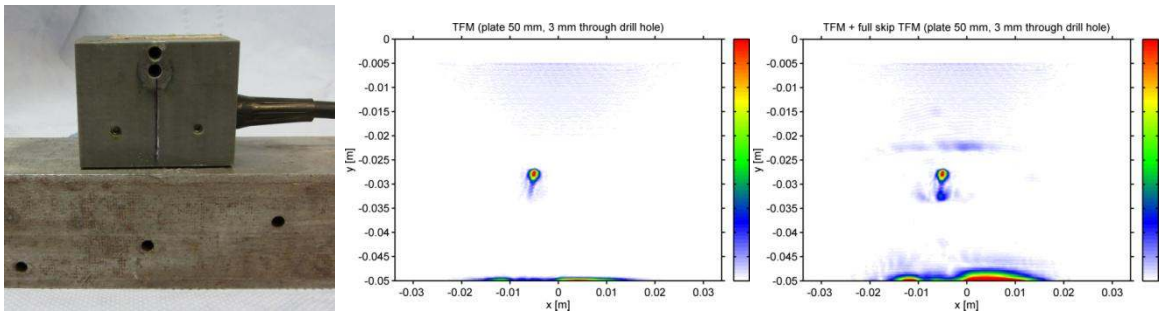

Figure 6: From left to right: TFM set up with the 64 elements phased array probe described in section 4, conventional TFM reconstruction, full skip TFM reconstruction. The steel block has a height of 50 mm and the through drilled holes have a diameter of 5 mm.

The mirroring at the backwall does only work for the full skip TFM. In case of the half skip TFM, one really has to deal with two different time-of-flights for the transmitting and receiving probe element, just as in the case of a circular backwall.

Half-Skip and Full-Skip TFM with a Circular Backwall

If the backwall is circular, the situation is much more complicated. The time-of-flight from a probe element to a grid cell including a backwall reflection does in general not coincide with the time-of-flight from the probe element to the grid cell mirrored at the backwall. Furthermore, the position of the corresponding virtual transducer changes with the probe element position. Therefore, for each probe element and grid cell combination we have to

compute the point on the backwall where the beam is reflected. If there is an additional water path, this reflection point on the backwall is also coupled to the intersection point on the interface between water and steel.

The computations of these reflection and intersection points have been implemented and first tested on the sample from Figure 6 by approximating the planar surface with a large circle radius of 10 m. The results (cf. Figure 7) are very similar to those from Figure 6. Verification of this code on a real pipe segment and the half skip TFM are currently work in progress.

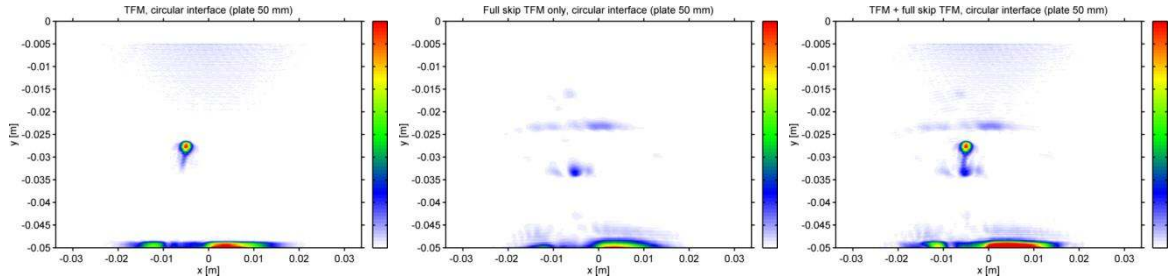

Figure 7: TFM reconstructions with circular interfaces on the sample from Figure 6, from left to right: conventional TFM reconstruction, reconstruction with full skip only, sum of both conventional and full skip reconstruction (= full skip TFM).

9. Defect Sizing

The sizing of defects in a reconstruction image is a difficult problem, because in the conventional TFM approach only that side of a reflector is reconstructed which faces the probe. Hence, methods like 6 dB drop only measure the size of this reflecting side, general conclusions to the real defect shape beyond that side are difficult. For special defects more detailed statements can be possible, e.g. in [14] and [15] the authors deal with the sizing of crack like defects in SAFT and TFM reconstructions.

Figure 8 shows the reconstruction of flat bottom holes whose bottom surface perfectly reflects the ultrasonic waves. In this case, the sizing of the defect with the 6 dB drop method is appropriate. For unknown defect shapes reconstructions from as many sides as possible would be ideal. But as the access to the specimen is often limited (e.g. in the pipe weld inspection) this will only rarely be possible. Here, the usage of half skip and full skip TFM will be helpful. Currently, we're working on defect sizing, too.

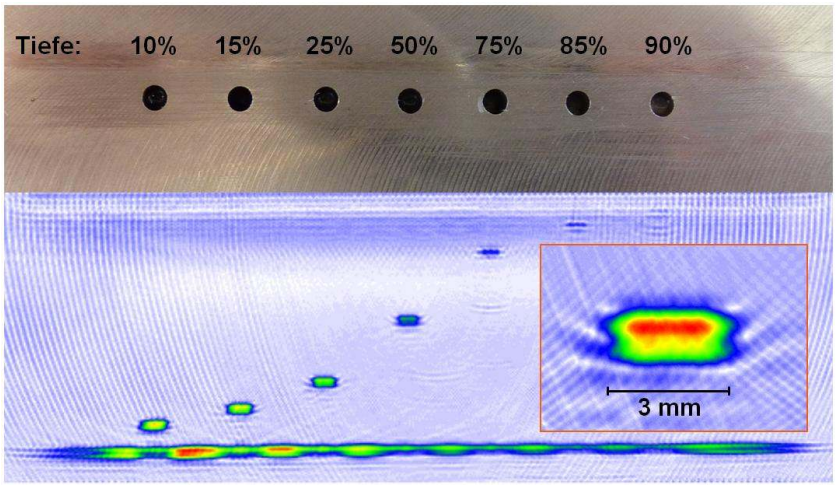

Figure 8: Reconstruction of flat bottom holes of 3 mm diameter and different depths. The red framed region shows a more detailed reconstruction of the 50% flat bottom hole. Here, the sizing with the 6 dB drop method would be possible.

10. Discussion and Outlook

In this paper, we presented the status of the SZMF TFM implementation. Our main (but not only) interest lies in the inspection of pipes, weld seams, and plates where anisotropic materials, curved surfaces, and other requirements are present. For a time efficient reconstruction the computational core has been implemented in CUDA C and probe sparsity can be used. Validating the half skip and full skip TFM also for curved surface and the sizing of defects is currently work in progress.

References

[1] Holmes, C; Drinkwater, B. W.; Wilcox, P. D.: Post-processing of the full matrix of ultrasonic transmit-receive array data for non-destructive evaluation. NDT & E International, Vol. 38, No. 8, 01.12.2005, p. 701-711.

[2] Wilcox, P. D.: Ultrasonic Arrays in NDE: Beyond the BS-Scan. Review of Progress in Quantitative Nondestructive Evaluation, Volumes 32A and 32B., 2013. p. 33-50 (AIP Conference Proceedings; Vol. 1511).

[3] Dominguez, N; Ithurralde, G.: Ultra-Fast Ultrasonic Inspection for Aeronautical Composites Using Paintbrush Acquisitions and Data Processing on GPU, www.ndt.net, 2010

[4] Sutcliffea, M.; Weston, M.; Dutton B.; Charlton, P.; Donne, K.: Real-Time Full Matrix Capture for Ultrasonic Non-Destructive Testing with Acceleration of Post-Processing through Graphic Hardware, NDT & E International, Volume 51, October 2012, Pages 16–23

[5**]** Moreau, L; Hunter, A. J.; Drinkwater, B. W.; Wilcox, P. D.: Efficient Data Capture and Post-Processing for Real-Time Imaging Using an Ultrasonic Array, Review of Progress in Quantitative Nondestructive Evaluation, Volume: 29, 07.2009, (AIP Conference Proceedings; Vol. 1211, No. 839).

[6] Moreau, L; Drinkwater, B. W.; Wilcox, P. D.: Ultrasonic Imaging Algorithms with Limited Transmission Cycles for Rapid Nondestructive Evaluation. In: IEEE Transactions on Ultrasonics, Ferroelectrics and Frequency Control, Vol. 56 (9), 09.2009, p. 1932 - 1944.

[7] Rubbers, P.: Ultrasonic Modelling, Using the Huygens-Fermat Principle, Talk in ModellingNDT 2007, Cape Town (South Africa)

[8] Weston, M.; Mudge, P.; Davis, C.; Peyton, A.: Time Efficient Auto-Focussing Algorithms for Ultrasonic Inspection of Dual-Layered Media Using Full Matrix Capture. In NDT & E International Vol. 47, 04.2012, p. 43-50

[9] Zhang, J.; Hunter, A. J; Drinkwater, B. W; Wilcox, P. D.: Monte Carlo Inversion of Ultrasonic Array Data to Map Anisotropic Weld Properties. IEEE Transactions on Ultrasonics, Ferroelectrics, and Frequency Control, Vol. 59, No. 11, 11.2012, p. 2487-2497.

[10] Harvey, G.; Tweedie, A.; Carpentier, C.; Reynolds, P.: Finite Element Analysis of Ultrasonic Phased Array Inspections on Anisotropic Welds. Review of Progress in Quantitative Nondestructive Evaluation: Volume 30A; Volume 30B, (AIP Conference Proceedings; Vol. 1335).

[11] Felice, M.; Velichko, A.; Wilcox, P. D.: Accurate Depth Measurement of Small Surface-Breaking Cracks Using an Ultrasonic Array Post-Processing Technique. NDT & E International, Vol. 68, 12.2014, p. 105-112.

[12] Zhang, J; Drinkwater, B. W.; Wilcox, P. D.; Hunter, A. J.: Defect Detection Using Ultrasonic Arrays: The Multi-Mode Total Focusing Method. NDT & E International, Vol. 43, No. 2, 03.2010, p. 123 - 133.

[13] Hutt, T. D.; Simonetti, F.: Reconstructing the Back of a Defect from its Mirror Image, Review of Progress in Quantitative Nondestructive Evaluation Volume 29. (AIP Conference Proceedings, Volume 1211, p.742-749)

[14] Spies, M.; Rieder, H.: SAFT Ultrasonic Imaging and Sizing of Stress Corrosion Cracks in the Heat-Affected Zone of Welded Austenitic Pressurized Components. JRC Scientific and Technical Reports: Proceedings of the 8th International Conference on NDE in Relation to Structural Integrity for Nuclear and Pressurised Components, 29 Sep. - 1 Oct. 2010, Berlin, Germany

[15] Zhang, J.; Velichko, A.; Drinkwater, B. W.; Wilcox, P. D.: The Characterization of Crack-Like Defects Using Ultrasonic Images. Review of Progress in Quantitative Nondestructive Evaluation, Volumes 29A and 29B (AIP, 2010. p. 895-902).